

# Application of Scanning Electron Microscopy to X-ray Analysis of Frozen-hydrated Sections

## I. Specimen Handling Techniques

ALBERT J. SAUBERMANN, PATRICK ECHLIN, PATRICIA D. PETERS, and REINIER BEEUWKES III

*Department of Anaesthesia, Harvard Medical School at Beth Israel Hospital and C. Dana Research Institute, Boston, Massachusetts 02215; Department of Botany, University of Cambridge, Cambridge, England; and Department of Physiology, Harvard Medical School, Boston, Massachusetts 02215*

**ABSTRACT** X-ray microanalysis of frozen-hydrated tissue sections permits direct quantitative analysis of diffusible elements in defined cellular compartments. Because the sections are hydrated, elemental concentrations can be defined as wet-weight mass fractions. Use of these techniques should also permit determination of water fraction in cellular compartments. Reliable preparative techniques provide flat, smooth, 0.5  $\mu\text{m}$ -thick sections with little elemental and morphological disruption. The specimen support and transfer system described permits hydrated sections to be transferred to the scanning electron microscope cold stage for examination and analysis without contamination or water loss and without introduction of extraneous x-ray radiation.

X-ray microanalysis of frozen-hydrated tissue sections is potentially an ideal method for analyzing diffusible elements in tissues. This paper describes a practical method of specimen handling for quantitative x-ray analysis of fully frozen-hydrated tissue sections in scanning electron microscopes (SEM) fitted with energy dispersive x-ray detectors. The success of the method is based on advances in two areas. First, reliable preparative techniques were developed to provide flat, smooth, 0.5- $\mu\text{m}$ -thick sections with little elemental redistribution and morphologic disruption. Second, a specimen support and transfer system was developed that allowed sections to be transferred to the SEM cold stage for examination and analysis without contamination or loss of water and without introducing extraneous x-ray radiation sources.

### MATERIALS AND METHODS

Small tissue specimens (liver) were placed on the ends of copper chucks ( $4 \times 12$  mm) and rapidly quench-frozen in melting Freon 12 ( $-158^\circ\text{C}$ ). Larger specimens (renal papillae) were frozen unmounted in melting Freon 12 and placed in a three-point holder. Cryosections were cut using a new cryosectioning system<sup>1</sup> mounted on a Sorvall Porter-Blum (MT-2 microtome; DuPont Instruments, Sorvall Biomedical Div. Wilmington, Del.). The new cryosectioning system included: (a) large cryochamber, (b) continuous flow, constant-temperature

cooling system, (c) three-point holder, (d) transfer port, and (e) razor-blade knife holder fitted with antiroll plate.

The cryochamber (Fig. 1) was constructed of foam polystyrene sheets (2.5 cm thick), and attached to the microtome knife stage so that chamber and knife moved together in the horizontal plane. The chamber was cooled by a continuous flow of dry  $\text{N}_2$  gas at constant low temperature, which entered the chamber beneath a secondary floor 10 mm above the main chamber floor. The cold  $\text{N}_2$  gas was produced by boiling liquid nitrogen ( $\text{LN}_2$ ) in a pressurized 25-liter Dewar flask with an electrical immersion heater. Heat input, and hence gas flow rate, was adjusted by an autotransformer. Gas leaving the Dewar flask was reheated to the desired temperature by passing through an insulated resistor (Ohmite, 100  $\Omega$ , 225 W, #0904) connected to a separate autotransformer. Specimen temperature was estimated by using a thermistor mounted on the chuck assembly. All "cutting temperatures" were measured at this point.

Sections were cut with a single-edge razor blade (Plus Platinum; Schick, Inc., Westport, Conn.), mounted in a brass vise, which clamped the razor blade with 2-3 mm of the edge extended, and which incorporated an antiroll device consisting of a microscope slide held (in a movable mounting) with its edge parallel to the upper surface of the blade (Fig. 2). The angle and spacing of the antiroll plate was set before cooling the chamber and final adjustment was made just before sectioning. All sections were cut with the microtome advance set for 0.5- $\mu\text{m}$  section thickness, using manual drive at very slow speeds ( $<0.1$  mm/sec) during the cutting portion of the cycle. The knife was set at a  $6^\circ$  clearance angle and the final cutting angle was approximately  $30^\circ$ .<sup>2</sup> Sections were cut singly and immediately placed on a cooled ( $-155^\circ\text{C}$ ) specimen holder by means of a cooled eyelash mounted on a wooden applicator stick.

<sup>2</sup> Because the final edge is hollow-ground, the final angle is  $25^\circ$  measured as the inclusive angle between tangents 1.5  $\mu\text{m}$  from the final edge.

<sup>1</sup> A commercial version of this system is now under development (J. Stella Enterprises, Amherst, N. H.)

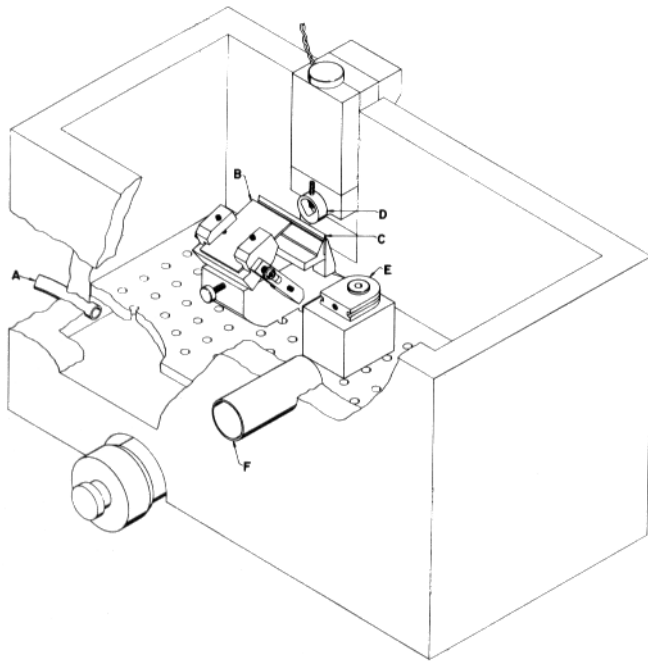


FIGURE 1 Schematic drawing of cryochamber showing relative positions of constant temperature N<sub>2</sub> gas inlet (A), knife holder with glass antiroll plate (B), razor blade in knife vise (C), three-point specimen chuck (D), specimen holder assembly (E), and transfer port (F).

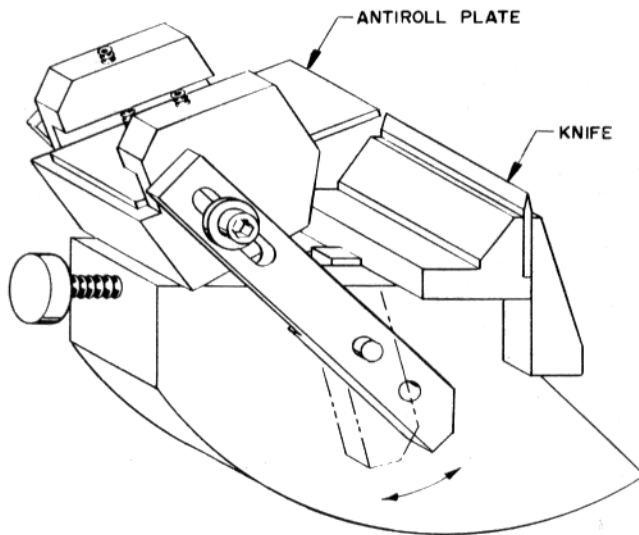


FIGURE 2 Schematic drawing of knife holder with antiroll plate retracted.

During sectioning, the section holder, mounted in a grooved transporter, rested upon a support partially immersed in LN<sub>2</sub> and was covered with a small polystyrene lid to prevent condensation. The section holder itself (Fig. 3) consisted of a beryllium (Be) cylinder 10 mm in diameter with a central 3-mm hole. The underside of the cylinder was cut away, leaving only a thin edge surrounding the 3-mm opening, as suggested by Gupta et al (9). A 75-mesh, 3-mm Be grid (Ted Pella, Inc., Tustin, Calif.) was centered over the hole, and the grid and the holder covered with a thin (100-nm) nylon film coated with 10 nm of carbon by evaporation.

Sections were transferred from the microtome chamber to the SEM cold stage by use of a transfer system consisting of a closable vacuum-tight specimen chamber and a rod bearing a heat sink (Fig. 4). The heat sink, of copper (25 mm in diameter, 75 mm long), was attached to the stainless-steel rod by a plastic (Delrin) insulator. The closable specimen chamber consisted of a Delrin tube bearing a vacuum flange on one end and a sliding seal for the rod on the other. The opening in the flange could be closed with a Delrin plug. In use, the heat

sink was cooled in LN<sub>2</sub>, after which it was quickly withdrawn into the protective Delrin tube and the transfer system brought to the microtome chamber. By fitting the transfer tube over the port of the chamber, the dry N<sub>2</sub> in the chamber replaced the ambient atmosphere in the transfer tube. The heat sink was then extended into the microtome chamber. The end of the heat sink (Fig. 4) was provided with a screw that engaged a thread in the grooved transporter (Fig. 3). The heat sink, with attached transporter, was then rapidly withdrawn into the Delrin tube and the plug inserted into the flange. By mating the flange of the transfer system to the airtight of the SEM, the transfer system was evacuated. The plug in the flange was removed by differential pressure during evacuation. The heat sink was then extended, carrying the grooved transporter to the precooled microscope cold stage.

The microscope cold stage and electron detector have been described previously (22). Stage temperature during operation was between -170° and -175°C. An opening in the stage permitted collection of transmitted electrons by a photodiode (#SG-100A; EG & G, Inc., Electro-Optics Div., Salem, Mass.) mounted ~35 mm below the specimen surface.

Examination and analysis was carried out on an AMR 900 SEM (AMRay, Burlington, Mass.), with a KeveX model 5100 energy-dispersive x-ray analysis system (10-mm<sup>2</sup> detector mounted at 30° tilt, resolution 155 eV FWHM; KeveX Corp., Foster City, Calif.). The system was equipped with time/rate interface (#5140) and x-ray mapping modules (#4945 and #4800) and was interfaced to a minicomputer (PDP 11/03; Digital Equipment Corp., Maynard, Mass.). The x-ray mapping output was shaped and displayed on a storage oscilloscope (R5115

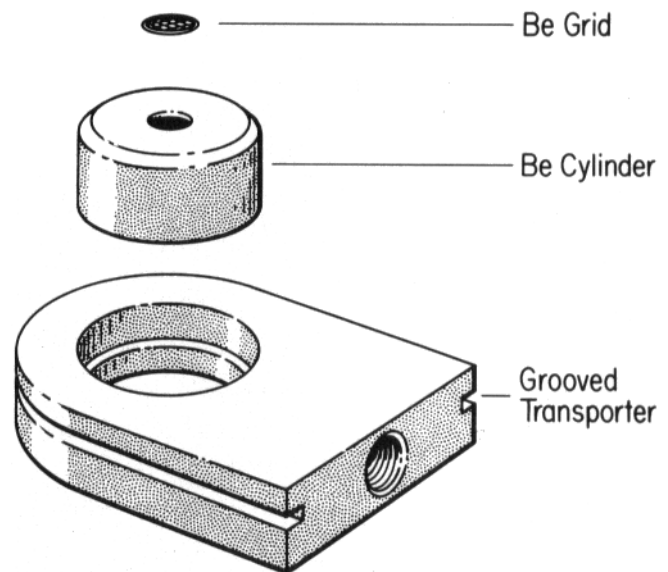


FIGURE 3 Exploded view of complete specimen holder assembly. This included beryllium (Be) grid, Be cylinder, and grooved transporter. The tapped hole on the grooved transporter (right-hand face) permits connection to the transfer system heat sink.

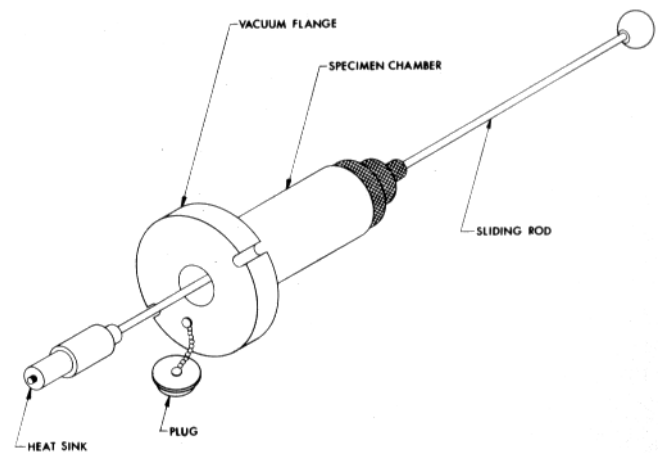


FIGURE 4 Schematic drawing of sealable transfer system with heat sink shown in extended position. The Delrin cylinder, with transparent vacuum flange, can be sealed with the small attached plug.

with 5A18N dual-trace amplifier and 5B10N time-base/amplifier; Tektronix, Inc., Beaverton, Oreg.). Probe current was measured directly from a Faraday cup fitted to the cold stage, using a picoammeter (Keithley 410A; Keithley Instruments, Inc., Cleveland, Ohio). Stage temperature was monitored adjacent to the transporter mount with a copper-constantan (Cu/Con) thermocouple connected to a digital thermometer (2160A-T; Omega Engineering, Inc. Stamford, Conn.).

For specimen imaging and x-ray analysis, the SEM was operated at 30-keV accelerating voltage, and 0.1-nA probe current. Each specimen was surveyed immediately after transfer into the SEM to assess suitability for analysis. Acceptance was based on the following criteria: (a) absence of surface relief and lacelike structures indicative of dehydration, (b) absence of curling, (c) position on the support film, and (d) absence of interfering frost crystals on the film surface or specimen. All analyses were carried out with a square raster whose size varied with compartment size and magnification, but was generally 1–20  $\mu\text{m}$  in width. Thus current density was between  $2.5 \times 10^{-5}$  and  $10^{-2}$  A/cm<sup>2</sup>. X-ray spectra were accumulated for constant live time intervals (30–100 s) in each experiment. A "top hat" digital filter was used to suppress background (23, 24, 29). The Hall method of analysis (11, 18) was used for quantitation. Continuum radiation (proportional to mass) was measured by integrating counts from the energy range of 4.60–6.00 keV inclusive. Characteristic x-rays of elements of interest were measured within the following fixed keV energy ranges at 20 eV/channel: sodium, 0.96–1.12 keV; phosphorus, 1.92–2.08 keV; sulfur, 2.24–2.40 keV; chlorine, 2.52–2.68 keV; potassium, 3.24–3.40 keV; calcium, 3.60–3.76 keV; iodine, 3.84–4.06 keV; and iron, 6.30–6.48 keV.

To define optimal sectioning conditions, pieces of mouse liver (CD-1, 200-gm males, Charles River Laboratories, North Wilmington, Mass.) were rapidly frozen in melting Freon 12 and cryosectioned at  $-80^\circ$ ,  $-50^\circ$ , and  $-30^\circ\text{C}$ . Sections (0.5- $\mu\text{m}$  thick) were cut, transferred to the SEM in the frozen-hydrated state, and examined in secondary mode. The sections were then freeze-dried in the SEM by raising the stage temperature, and reexamined in the scanning transmission (STEM) mode. Topographical features produced during sectioning were studied to determine the effect of cryosectioning temperature on morphology.

To define optimal sample support, x-ray continuum was measured from experimental section holders with different hole configurations and with and without the use of Be grids. Temperature rise at the section plane was determined by a Cu/Con thermocouple made from 0.001-inch-diameter wire (#COCO-001; Omega Engineering, Inc.) soldered to a 1.3-mm length of 0.010-inch-diameter Cu wire. (Total weight of wire + 1-cm length of thermocouple wire was 0.00096 g.) The calibrated thermocouple and wire was placed on the surface and in the center of carbon-coated nylon-covered specimen holders with and without Be support grids. A heat source at  $56^\circ\text{C}$  (electric wax spatula, HR Superior #17-037) was vertically positioned 2 mm from the middle of the specimen holders. The temperature of the thermocouple assembly was recorded for a 3-min period. The temperature of a Cu grid lying in the section plane was also measured during simulated transfers.

To determine the relationship between secondary or STEM image features and specimen hydration state, nominal 0.5- $\mu\text{m}$ -thick rat renal papilla sections, cut at  $-30^\circ\text{C}$ , were examined before and after drying in the SEM. To define optimal criteria for compartment identification, we made correlations between secondary, STEM, and x-ray mapping images of single sections before and after drying, employing images at magnifications of 500–10,000, and evaluated element maps for Na, K, Cl, S, and P.

To test the suitability of these specimen-handling techniques for direct elemental analysis of frozen-hydrated sections, x-ray peak-to-continuum ratios were measured in defined compartments in both hydrated and dried sections.

## RESULTS

### *Cryosectioning and Transfer*

The temperature of the tissue block was found to be a major factor in successful cryosectioning of 0.5- $\mu\text{m}$ -thick sections. Smooth, flat, 0.5- $\mu\text{m}$ -thick sections were consistently produced at  $-30^\circ$  to  $-40^\circ\text{C}$ . Such sections could be cut individually and transferred to the section holder. Without the use of the antiroll plate, sections curled and could not be attached to the grid for transfer. Secondary and STEM images of mouse liver sectioned at  $-80^\circ$ ,  $-50^\circ$ , and  $-30^\circ\text{C}$  are shown in Fig. 5A–C, respectively. At  $-80^\circ\text{C}$ , sections were rough, showing definite evidence of discontinuous chip formation with overlap. Morphology was distorted and cellular components unrecognizable. At  $-50^\circ\text{C}$ , sections were still unsatisfactory, exhibiting some fracturing features. Morphological compartments were clear but still distorted (Fig. 5B). At  $-30^\circ\text{C}$ , sections were smooth and

flat. Morphological detail was suitable for compartment identification (Fig. 5C). At high magnification, it was possible to distinguish nuclei, nucleoli, and cell boundaries in such sections (Fig. 6).

Although ice crystals could not be seen in frozen-hydrated sections, in dried sections ice-crystal damage was visible as voids (0.2–0.6  $\mu\text{m}$  in the longest dimension) in the tissue matrix. Ice-crystal-damage artifacts varied from one compartment to another and appeared to have been introduced during initial freezing or sectioning, as no increase in ice-crystal-damage artifact was observed during maintenance of hydrated sections in the SEM at  $-175^\circ\text{C}$  for 3–4 h. No visible contamination by pump oil, or accumulation of frost occurred.

The described configuration of the Be support stub together with the use of a Be grid and carbon-coated nylon film was found necessary to provide good thermal conductivity and low continuum generation without introduction of extraneous characteristic peaks. Fig. 7 shows the improvement in continuum resulting from enlargement and chamfering of the edge of the internal bore of Cu specimen holder. The addition of a Be grid to a Be holder added no significant continuum except in the region over, or within, 5  $\mu\text{m}$  of a grid bar. Temperature-rise experiments showed that addition of the Be grid significantly improved thermal conductivity (Fig. 8).

During sectioning, the tissue block and sections on the knife were presumably at chamber temperature. Placement of sections on the cooled holder within the chamber lowered their temperature to about  $-150^\circ\text{C}$ . During subsequent transfer steps, using the precooled transfer system, the measured temperatures never rose above  $-145^\circ\text{C}$ , and fell to  $-167^\circ\text{C}$  when the grooved transporter was in position on the SEM cold stage. Using these sectioning and transfer procedures, only 5% of the sections transferred failed to meet the hydration criterion. Only 10% were found unsuitable for analysis, based on criteria of hydration, flatness, position, and frost.

### *Imaging and X-ray Analysis*

Secondary and STEM images of hydrated sections had few recognizable morphological features (Fig. 9A and B). When partially or completely dried, distinct surface features became visible (Fig. 9A). Ice-crystal-damage artifacts appeared in the tissue matrix as lacelike patterns (Fig. 10A–D).

Frozen-hydrated sections maintained at  $-175^\circ\text{C}$  were studied for up to 4 h without change in image or change in continuum x-ray count rates. Loss of water during drying was associated with improved STEM images (Figs. 9A and 10A–D). However, the presence of recognizable structures in the STEM mode was dependent upon both state of hydration and section thickness. Fig. 11A shows STEM images of two adjacent and serially cut frozen-hydrated sections of rat renal papilla (sections 1 and 2). Both hydrated sections had similar elemental mass fractions in similar compartments, yet compartment identification in the STEM mode was possible in section 1 and not section 2. As measured by greater electron density and mass (i.e., continuum counts) section 2 was thicker than section 1.

X-ray mapping of selected elements provided a useful aid for compartment identification in frozen-hydrated sections. In renal papilla, for example, phosphorus was present in highest levels in nuclear compartments, but was less in cytoplasm, and still less in extracellular matrix. Although contrast was low in the hydrated sections, maps suitable for preliminary compart-

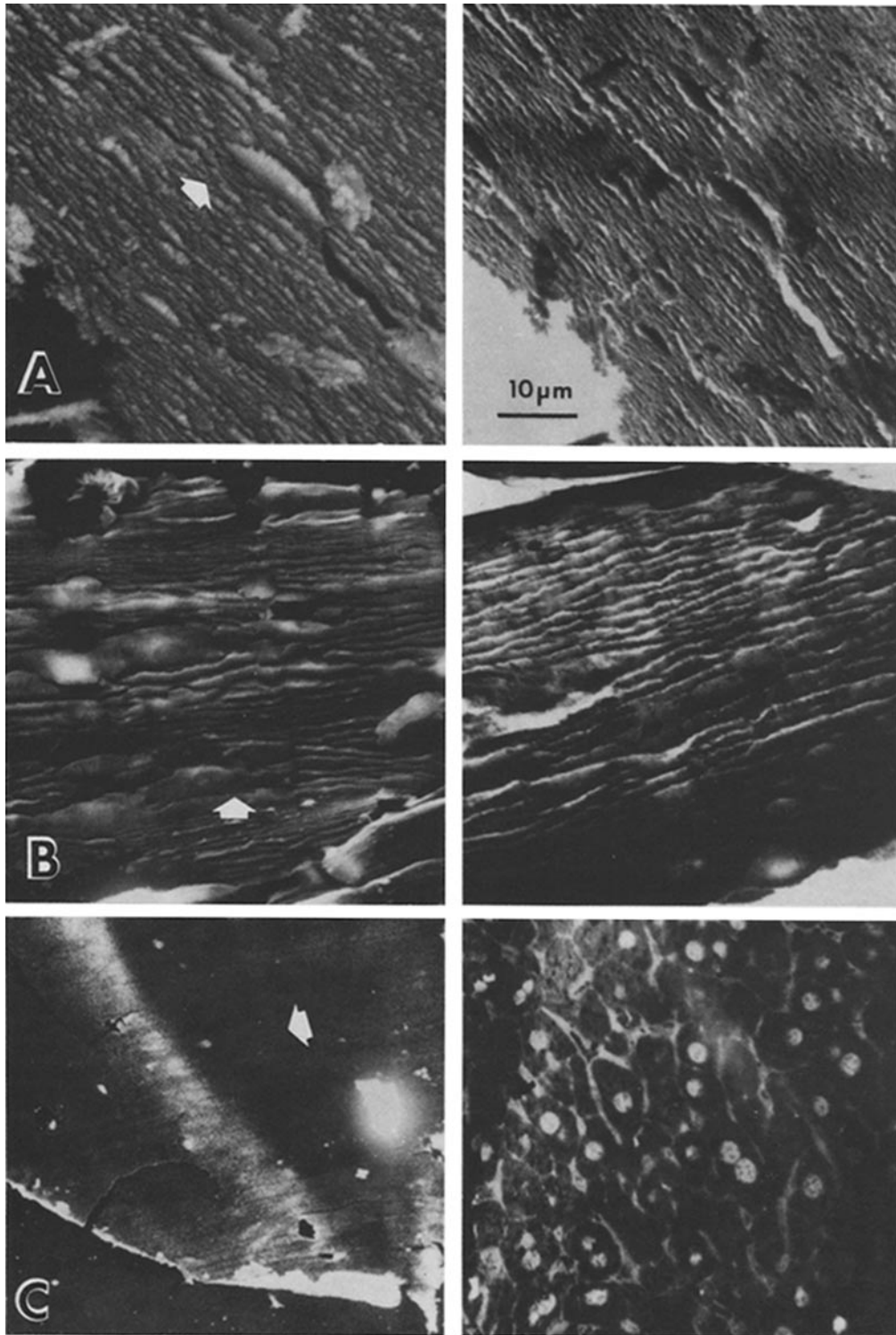


FIGURE 5 Secondary (left) and transmitted electron (right) images of 0.5- $\mu\text{m}$ -thick sections of mouse liver cut at  $-80^{\circ}\text{C}$  (A) obscure morphologic detail. Sections cut at  $-50^{\circ}\text{C}$  (B) show continuous chips beginning to form, but morphological detail is still unclear. In the continuous chip formed at  $-30^{\circ}\text{C}$  (C) under low work conditions, morphological detail is easily seen. Arrows indicate cutting direction.

mental identification could be made. Fig. 12A and B shows phosphorus elemental maps of a rat renal papilla section in hydrated (A) and dried (B) states together with a STEM image (Fig. 12C) of the same region.

By spectral analysis, we observed characteristic x-ray peaks of Na, Mg, P, S, Cl, K, Ca, and Fe and calculated peak-to-continuum ratios in both hydrated and dry states (Table I).

Different compartments had different elemental compositions. In sections of renal papilla, compared with interstitial space, collecting-duct cytoplasm was lower in Na, Cl, and S, similar in K, and higher in P. Interstitial cells contained more Na and Cl than collecting-duct cells. Interstitium was higher in S than cells were. When specimens were dried in the instrument, mass fractions increased in all compartments, indicating that the

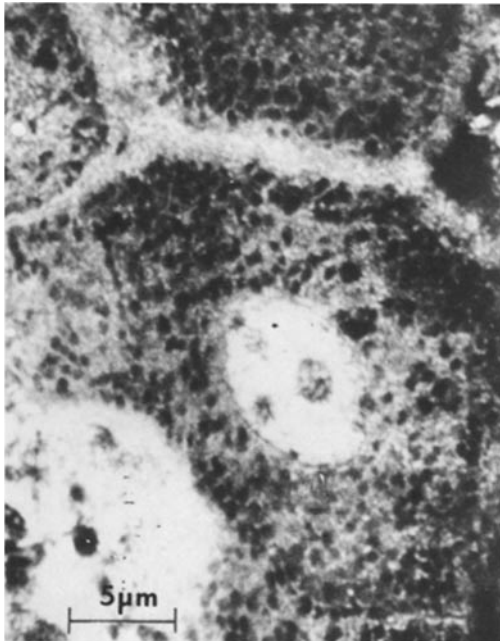


FIGURE 6 Scanning transmission image of frozen dried mouse hepatocytes. This 0.5- $\mu\text{m}$  section was cut at  $-30^{\circ}\text{C}$ . Distinct nuclear and cellular boundaries are visible.

differences observed were not entirely attributable to differences in the size of compartmental water spaces (19). Thus, direct elemental analysis was practical for specimens prepared and handled using these techniques.

## DISCUSSION

Several methods describing application of x-ray microanalysis to freeze-dried cryosections for diffusible element localization by use of both SEM and STEM have been reported (1, 3, 5, 24, 25, 27, 28, 31). In 1974, Moreton et al. (16) first demonstrated the feasibility of direct x-ray analysis of frozen-hydrated tissue sections in the SEM. Saubermann and Echlin (20) later developed improved methodology for such analysis. Gupta et al. (9) adapted and improved these methods for use with a microprobe instrument fitted with wavelength and energy-dispersive detectors. Although these techniques can analyze frozen-hydrated sections, two major problem areas have precluded reliable and general application. First, the cryosectioning process was poorly understood and it was impossible to cut uniform, fully hydrated sections consistently with available sectioning apparatus. Second, there was no simple system for specimen support, transfer, and maintenance at low temperature within the instrument (10). These problems appear to have been solved by the techniques described here.

### Cryosectioning

Cryosectioning must produce smooth, relatively thin, flat tissue sections. Frozen sections nominally 0.5- $\mu\text{m}$  thick are thin enough to permit the Hall analytical method (11, 18) to be used and to show reasonable morphology, using STEM imaging at 30-keV accelerating voltage. Such sections are thick enough to provide sufficient characteristic x-ray intensity for energy-dispersive analysis with reasonable counting rates at a reasonably small probe current. Cutting such sections is difficult; frozen biological tissue appears to behave much as brittle metals do during cutting, thus making cryosectioning funda-

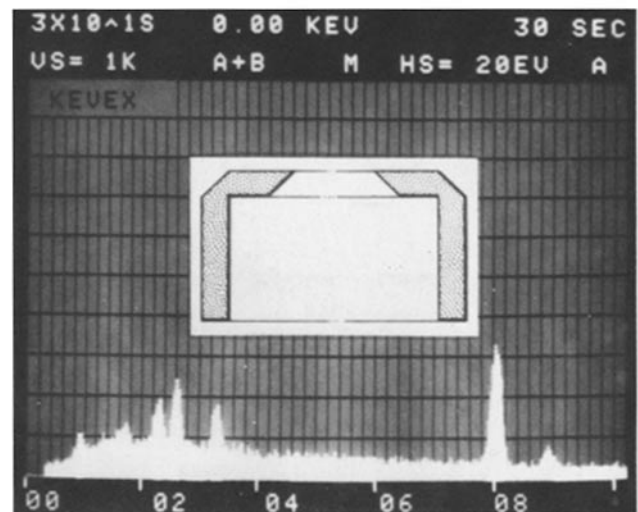
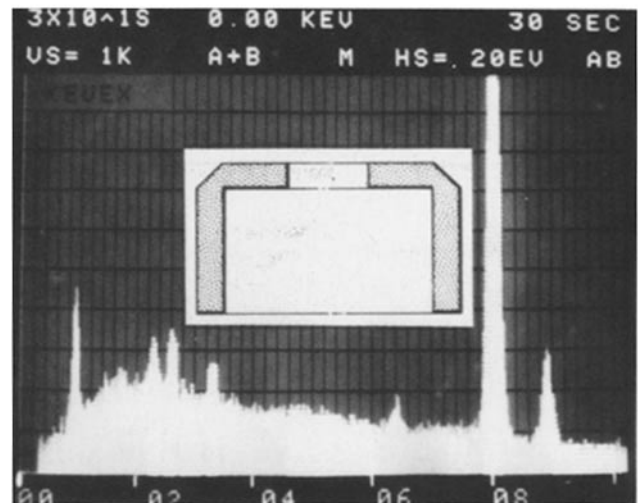
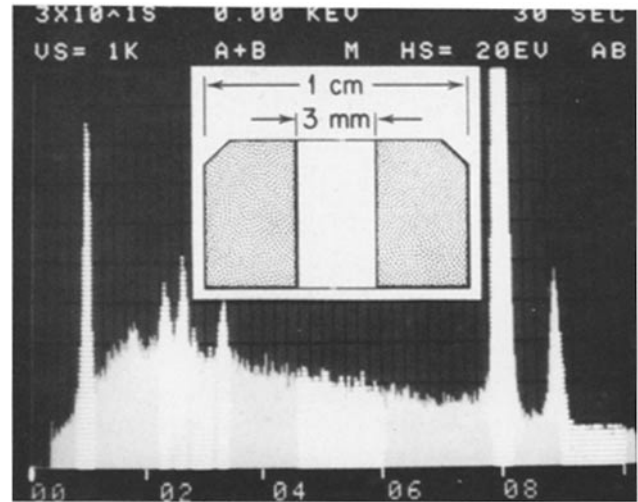


FIGURE 7 X-ray spectrogram obtained during evaluation of specimen support cylinders having the configuration shown. To determine support-cylinder characteristic x-ray and extraneous continuum contribution, KSCN standards were mounted on nylon film supported by copper cylinders of different internal configurations. When the interior of the cylinder was cut away and the edge of the opening tapered (bottom), characteristic copper x-ray production (peak above 8.0 keV) was minimized, and the extraneous continuum substantially reduced. This improved the peak-to-background ratios of the sulfur (2.3 keV) and potassium (3.0 keV) peaks (see text).

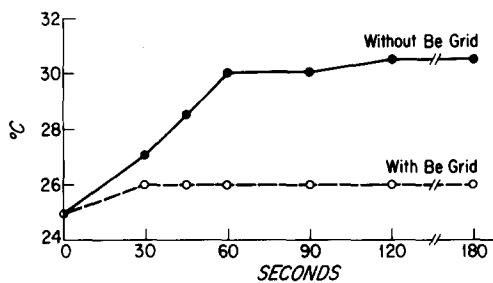


FIGURE 8 Temperature measured on nylon film surface with and without Be grid support during a 3-min exposure to a radiant heat source. The improvement resulting from the use of Be support grids was substantial.

mentally different from plastic- or paraffin-section cutting. During metal-cutting operations, internal stress is created at the cutting-tool edge; the concentration of these stresses cause the chip to shear from the material and flow along the chip/tool interface (15). This separation occurs through plastic deformation or through fracturing, depending upon the ductility of the metal. If fracturing occurs, discontinuous chips are formed. If plastic deformation occurs, a continuous chip is formed (15). As the angle between the top of the tool and the face of the workpiece is narrowed, chip deformation in the shear zone is reduced. Such conditions promote continuous chip formation.

Application of these metal-cutting principles to cryosectioning required reducing the knife angle as much as possible. By using a razor blade having a knife angle of  $\sim 25^\circ$  at a  $6^\circ$  clearance angle, sections were cut with a total angle of only  $31^\circ$  between the top of the knife and the block face. In contrast to glass knives, the relative flatness of the razor blade below the cutting edge prevented further curling and permitted use of a closely spaced antiroll plate. The antiroll plate opposed deformation near the shear zone so that flat continuous chips were formed. In addition to their morphological advantage, smooth, flat sections provided a larger surface area in contact with the support film. Such sections rarely came off the specimen holder or were dislodged during transfer. Thus it proved unnecessary to use glue (17), pressure (9), capping grids (14), or second films (5) to hold the section in place.

The brittleness of frozen biological tissue depends upon its composition, structure, and temperature. Ice per se is very hard and brittle, thus it is not surprising that tissue containing many large ice crystals should section poorly, forming discontinuous chips. Ice-crystal size has been found to be related to fractional water content within the tissue (2, 18). Although this factor is not controllable, efforts to reduce ice-crystal formation during initial freezing are likely to be of benefit to cryosectioning (6, 7, 26). Similarly, although the structural distribution of relatively hard and soft regions also has a major effect on cutting work (21), this factor is also beyond the experimenter's control. The major controllable factor appears to be temperature. As shown in Fig. 5A-C, mouse-liver cryosections formed discontinuous chips when cut at  $-80^\circ\text{C}$ . Continuous chip formation began at  $-50^\circ\text{C}$ , and the entire section was a continuous chip when cut at  $-30^\circ\text{C}$ . Clearly, more morphological information is obtained with continuous chips, and the origin of the x-ray signal is well defined.

The effective cutting temperature depends upon both chamber temperature, which defines the initial temperature of the block face (4) and upon the heat introduced during sectioning. During metal machining, heat is produced by friction as the chip slips along the cutting-tool face, and by plastic deforma-

tion occurring as the chip is formed. The temperature rise in the chip and workpiece varies primarily with composition of the workpiece, rate of cutting, and type of chip formed (21). In a previous study of cutting work during cryomicrotomy, it was found that the total amount of heat introduced increased markedly as sectioning temperature became colder (21). This heat input results in a temperature rise of both section and block. Thus, sections cut at very low temperatures as measured on the block support, under conditions requiring high work inputs, may actually have been produced at relatively high effective cutting temperatures. Hodson and Marshall (13) claimed to have cut sections at  $\text{LN}_2$  temperature and Appleton (1) has noted that the optimal temperature for thin sectioning in his cryostat ranged from  $-70^\circ$  to  $-80^\circ\text{C}$  at 2 mm/s cutting speed. It is possible that under such conditions, the effective cutting temperature has been raised to the point at which the tissue is sufficiently ductile to allow continuous chips to be produced. As heat input is apparently independent of section thickness, potential temperature rise must vary inversely with section mass (21). Hence, thick sections do not rise in temperature as much during cutting as thin sections. We have observed that thick sections generally cannot be cut so as to form continuous chips at temperatures below  $-80^\circ\text{C}$  unless heat input is raised by cutting at faster speeds (21). In addition, if partial tissue dehydration has occurred before or after freezing, the tissue may have reduced brittleness and hence has improved cutting properties at very low temperatures.

Unlike other cryosectioning systems, the system described was designed to have all components at nearly the same temperature. This was achieved by cooling the chamber with a constant flow of  $\text{N}_2$  gas at regulated temperature. Such a continuous-flow cooling system was introduced by Christensen (4) in 1971; however, the reheating of  $\text{N}_2$  gas in his system occurred by passing it through an uninsulated tube. Hence, cryochamber temperature was regulated by changing gas-flow rate (4). Later commercial versions of Christensen's system attempted to regulate temperature by intermittent gas flow, effectively preventing attainment of thermal equilibrium. In the present system, component materials within the chamber were selected to speed the attainment of thermal equilibrium. The thermal conductivity of steel at  $-30^\circ\text{C}$  is nearly 40 times that of glass, hence the use of a steel blade helped prevent temperature rise at the cutting edge. Similarly, by having knife and block at the same temperature, thermal gradients during sectioning were reduced and section uniformity improved. The demonstrated success of this approach indicates that complex systems for separate regulation of knife and block temperature are not necessary. Indeed, since actual knife-edge and block-face temperatures are not measured by such systems, the "control" they offer is illusory.

The  $\text{N}_2$  gas used to cool the chamber could potentially remove water from cryosections. To prevent this, sections were placed on a precooled ( $-155^\circ\text{C}$ ) specimen holder immediately after cutting. This holder was then covered to prevent exposure to the flowing gas. At  $-30^\circ\text{C}$ , drying occurred within several minutes if the specimen was left exposed to anhydrous  $\text{N}_2$  unless these precautions were taken. At  $-40^\circ\text{C}$  the drying rate decreased, so that a section could be left safely for 5–10 min. Once cutting started, the entire process from cutting to transfer into the SEM was completed within 3–5 min.

#### Specimen Holder and Transfer

The specimen support system must provide good thermal conductivity for heat removal from hydrated sections without

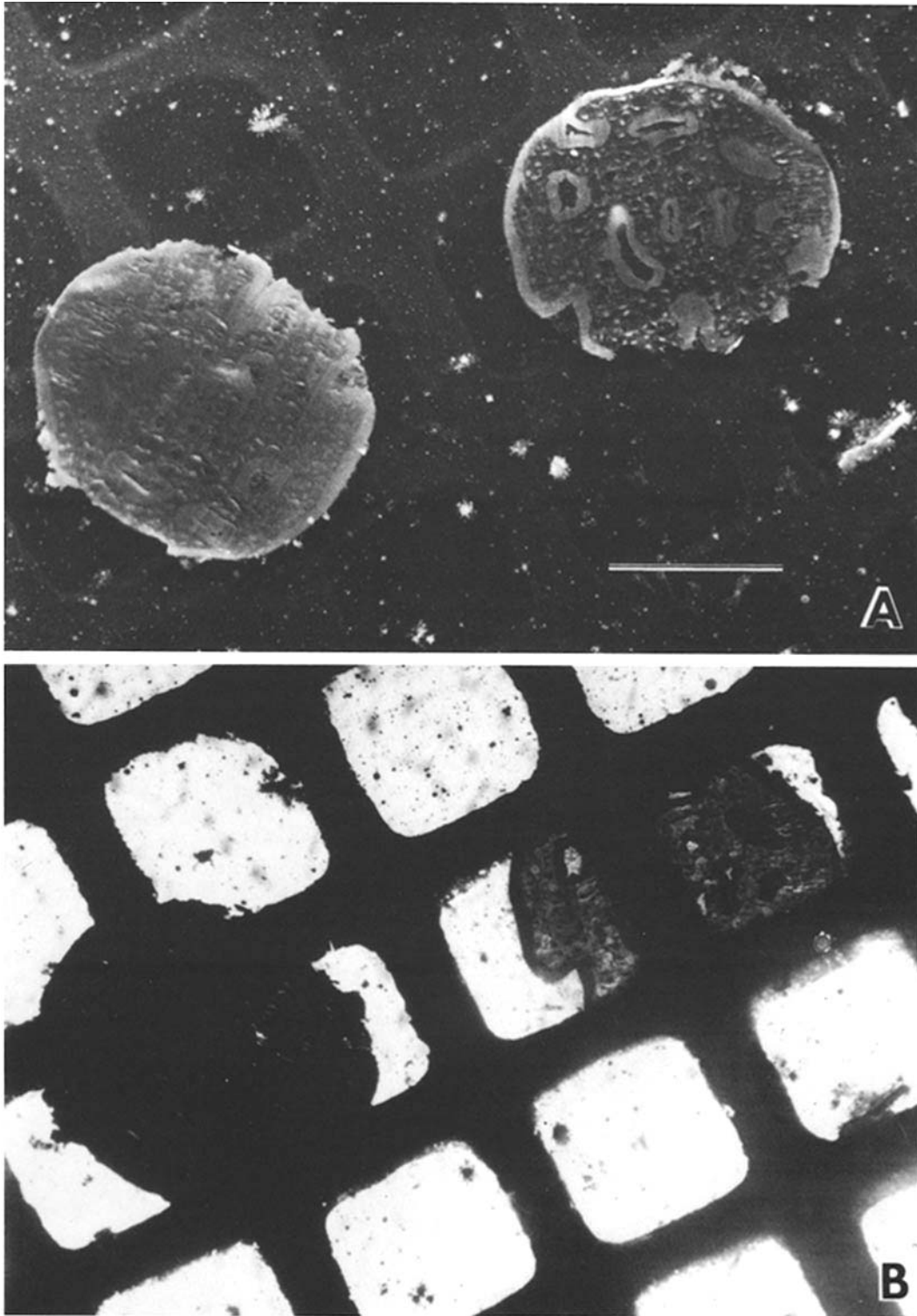


FIGURE 9 Frozen-hydrated (left) and frozen-dried (right) sections of rat renal papillae are shown in secondary (A) and STEM (B) images. Distinct collecting-duct cross sections are clearly seen in the dried sections. However, the nearly uniform density and the absence of topography in the frozen-hydrated section makes compartmental identification difficult. The adjacent hydrated and dried sections were obtained by allowing one section to dry in the microtome at  $-30^{\circ}\text{C}$ , by not cooling the specimen holder to  $-155^{\circ}\text{C}$ , and by leaving the section at  $-30^{\circ}\text{C}$  for  $\sim 45$  min. The specimen holder was then cooled to  $-155^{\circ}\text{C}$  and a second hydrated section added. The two sections were then transferred to the microscope cold stage. The background particles seen on the support film are frost. Bar, 0.3 mm.

itself becoming a source of extraneous radiation during x-ray analysis. In the present studies, these goals were best achieved by placing sections on a carbon-coated nylon film supported by a Be grid resting over a specially shaped opening in a Be

cylinder. The carbon coating on the nylon films was required to provide electrical conductivity. As Fuchs et al. (8) have shown, top coating was unnecessary when sections were supported on a conductive surface. The choice of nylon for the

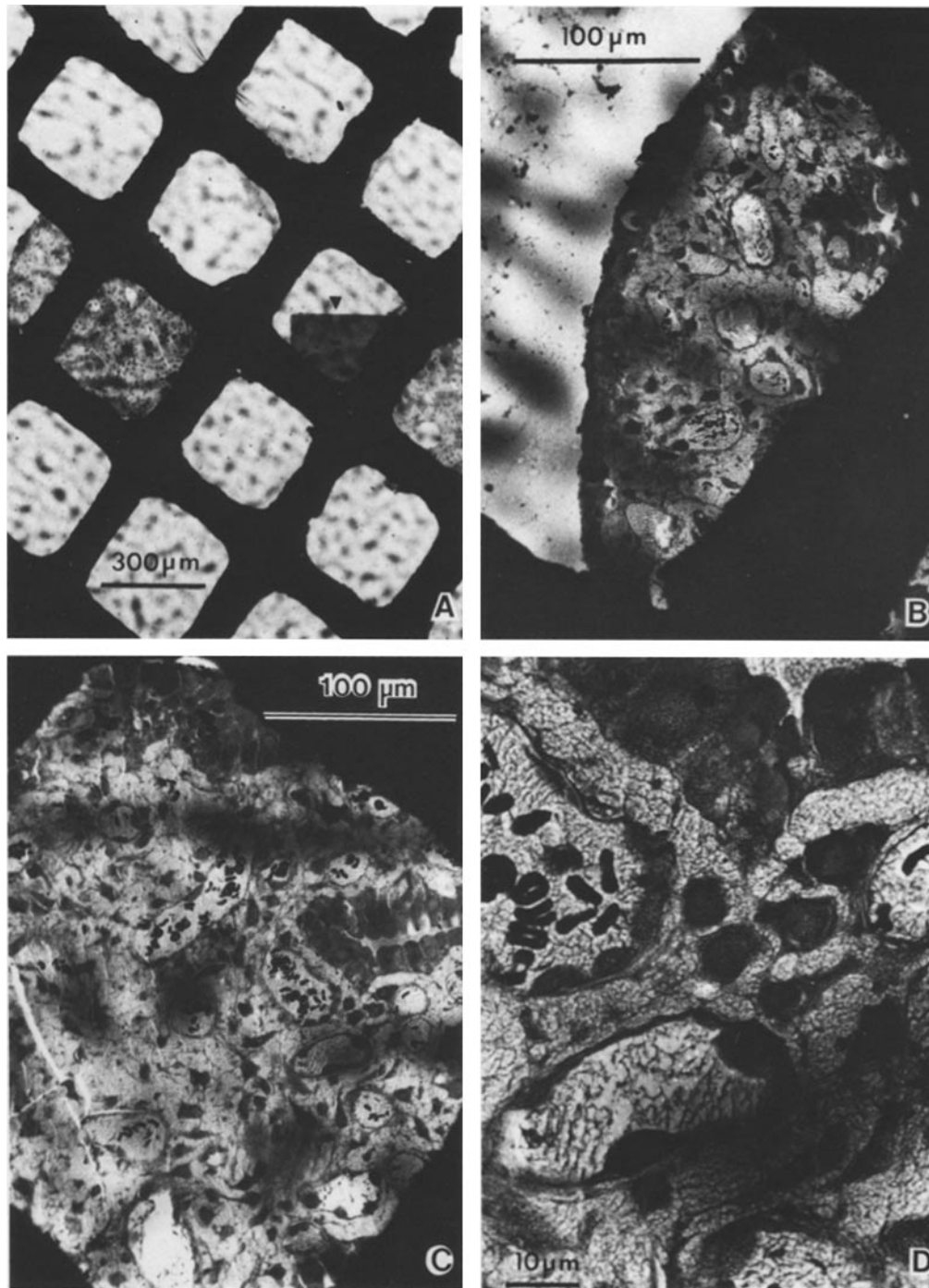


FIGURE 10 Scanning transmission images of rat renal papillae (from diabetes insipidus animal) showing distinct morphological compartments. Arrow indicates KSCN, resin-embedded standard.

support film was based on its superior durability under electron bombardment (12). The thermal resistivity of the supporting system was markedly reduced by the use of a 75-mesh Be grid beneath the nylon film. Although the thermal conductivity of Be is not as high as that of Cu, the use of Cu grids would introduce an unacceptably large extraneous x-ray background. For this reason, Be was also selected for the hollow cylinder supporting the grid. Although carbon was tried in this application, the metal was mechanically more stable and the shape of the opening could be controlled more precisely. Aluminum holders and aluminum-coated nylon films have been used for specimen support (9, 16, 20). However, a characteristic x-ray

signal of aluminum interferes with Na detection by the energy-dispersive analyzer. In addition, aluminum adds more extraneous background radiation than carbon. In our experience, frozen-hydrated sections placed on aluminum-coated nylon films without a grid support did not remain hydrated unless part of the section was located over the solid metal of the stub. The use of aluminum coating in place of carbon coating for the nylon film did not appear to improve thermal conductivity significantly.

For ease of handling, mechanical and thermal interfacing between the specimen holders and the microscope cold stage was provided by means of a grooved transporter fabricated

from Be. The specimen transfer system provided a closed, frost-free environment for this transporter and a massive heat sink to minimize temperature rise. This system maintained specimens at temperatures colder than  $-150^{\circ}\text{C}$  during transfer, and, because the Delrin tube was back-filled by cold dry  $\text{N}_2$  from the microtome chamber, frost accumulation during transfer was found to be negligible. The use of a plug removed by

differential pressure during airlock pumpdown eliminated the necessity for complex valving systems. This transfer system can potentially be adapted to any SEM by modification of the grooved transporter and the vacuum flange.

The microscope cold stage has been previously described (22). This was designed so as to incorporate an anticontamination system. Specimen temperature was maintained  $\sim 10^{\circ}$ -

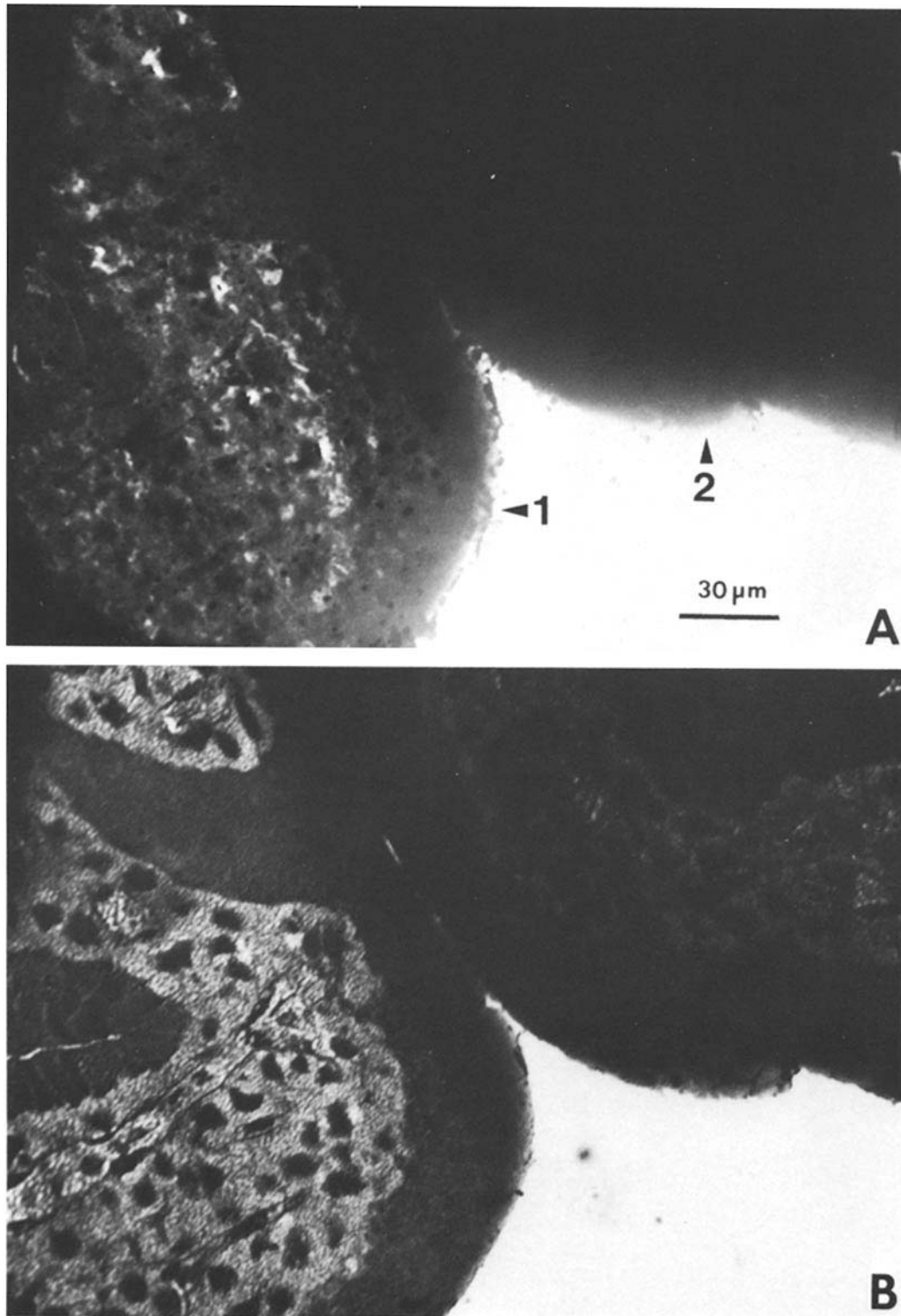


FIGURE 11 Fully frozen-hydrated sections of rat renal papillae (A) showing visible morphology in the thinner section (1) but not in the thicker section (2) with corresponding STEM image of same sections in the dried state (B). The presence of visible morphology in the hydrated state is not an absolute criterion of hydration but depends upon section thickness.

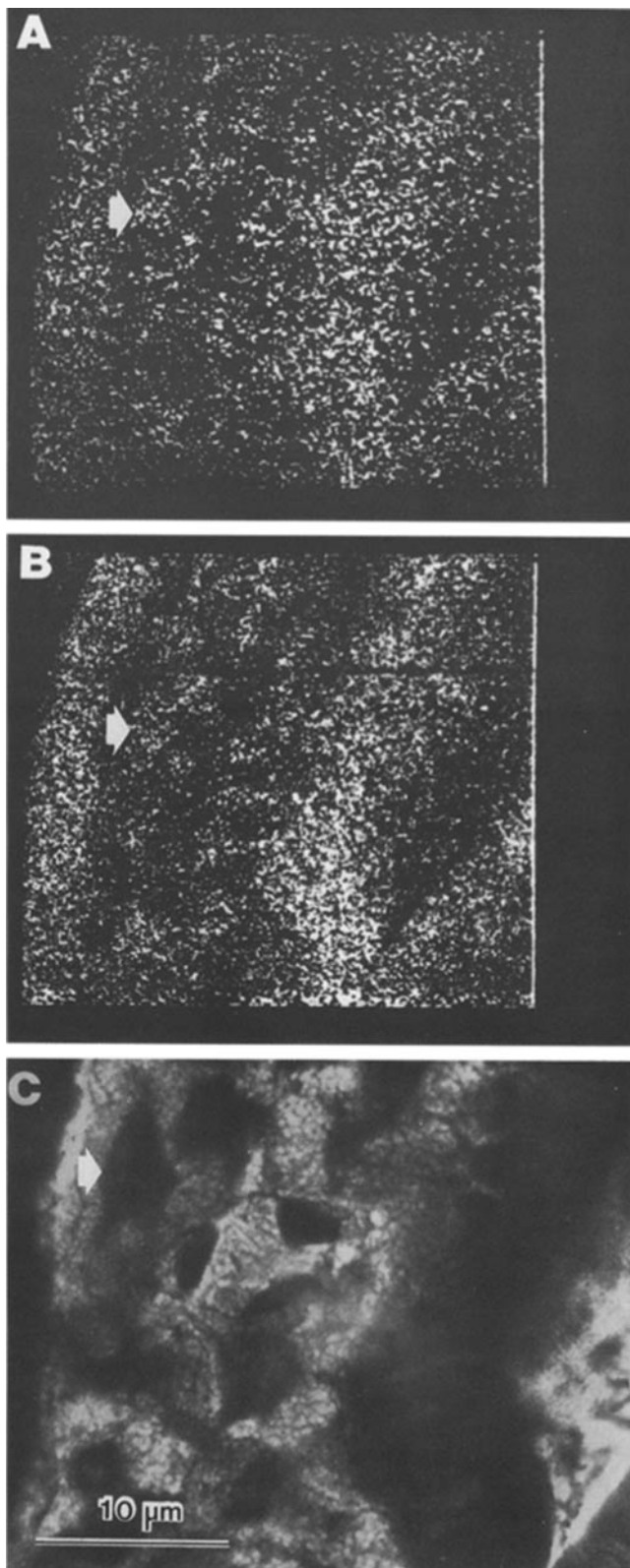


FIGURE 12 Phosphorus x-ray maps shown in hydrated state (A) and dried state (B) with STEM image of corresponding figure (C). The better peak-to-background ratios permit formation of a more distinct map in the dried state (B). This improvement in peak-to-background ratio in the dried section is associated with water loss caused by drying. Arrow points to interstitial cell nucleus.

15°C warmer than the surrounding cold surfaces. It should be recognized that if the section is maintained at too low a temperature it effectively becomes a part of the anticontamination system and may accumulate water, pump oil, or other contaminants. In practice, it was found that at stage temperatures below  $-150^{\circ}\text{C}$  the rate of ice sublimation from sections was so slow as to be undetectable. This was true despite the thermal input from radiation and from the beam. The total radiation emitted from the specimen chamber walls of a similar instrument has been estimated at 34 mW.<sup>3</sup> However, only a small fraction of this radiation impinges on the tissue section. Beam heating is of potentially greater importance. The total power of the 0.1-nA electron beam of 30-keV accelerating energy used in these studies is 3 mW. Because most electrons pass through the section, only a small fraction of this is absorbed. The absence of detectable heating effects found in these studies is in accord with the theoretical calculations of Talmon and Thomas (30) for similarly mounted 0.5- $\mu\text{m}$ -thick sections.

### Compartment Identification and Analysis

The identification of compartments in fully hydrated tissue sections was difficult. Theoretically, well-cut sections should show no surface topography except that arising from imperfections in the knife. However, secondary electron images provided some morphological information when differential shearing planes occurred in different tissue compartments. Transmitted electron images had little contrast. Thin, frozen-hydrated sections showed morphology that was not visible in equally hydrated thicker sections viewed simultaneously. Presumably, the larger signal passing through the thinner section permitted greater electronic contrast enhancement. Thus, although dried sections showed good contrast, the presence of a STEM image did not necessarily indicate dehydration. On the other hand, the presence of visible ice-crystal-damage artifacts, either in the STEM or secondary image, was invariably an indication of water loss.

To assist in compartment identification in hydrated sections, x-ray mapping techniques were employed. Although maps were prepared for many elements, only the map for phosphorus proved valuable for studies of renal papillae. Such a map corresponded roughly to the application of a nuclear stain. In other tissues, identification of cells by their relatively high K content was possible. Compartmental analysis performed on the basis of such maps could be confirmed through use of STEM images of the same area after drying. STEM images of frozen-dried sections showed clearly identifiable cellular structures. Intracellular organelles could not be identified with certainty because of ice-crystal damage. Such damage, presumably introduced during initial freezing steps, limits the application of this methodology. By freezing very small tissue specimens, Somlyo et al. (27, 28) have succeeded in high-resolution analysis of freeze-dried, ultrathin sections.

X-ray analysis of defined tissue compartments in frozen-hydrated specimens showed distinct and characteristic patterns of elemental distribution. Similar patterns were observed in sections after drying. Peak-to-background ratios were sufficient

<sup>3</sup> J. Norton (AMRay Corp.), personal communications. This calculation assumes that the chamber walls are uninterrupted flat surfaces at ambient temperatures.

TABLE I

Peak-to-Continuum Ratios Observed in Compartments of Frozen-hydrated and Frozen-dried Rat Renal Papilla

	Collecting-duct cells		Interstitial		Interstitial cells		Papillary epithelial cells	
	H	D	H	D	H	D	H	D
n	7	11	8	7	15	7	7	9
Continuum	12,203 ± 2,157	5,720 ± 453	10,953 ± 2,207	2,384 ± 578	10,862 ± 1,430	5,049 ± 219	12,215 ± 4,919	4,406 ± 576
Na	.013 ± .006	.079 ± .012	.019 ± .004	.175 ± .014	.026 ± .007	.204 ± .004	.014 ± .005	.065 ± .027
P	.103 ± .007	.331 ± .052	.025 ± .014	.070 ± .015	.060 ± .019	.173 ± .052	.116 ± .016	.366 ± .046
S	.018 ± .015	.042 ± .008	.024 ± .004	.121 ± .027	.017 ± .005	.034 ± .018	.018 ± .005	.043 ± .011
Cl	.141 ± .021	.394 ± .044	.155 ± .025	.652 ± .109	.228 ± .058	.833 ± .041	.122 ± .017	.388 ± .107
K	.088 ± .007	.244 ± .035	.043 ± .006	.169 ± .030	.060 ± .013	.165 ± .003	.099 ± .014	.267 ± .009

All values are expressed as means ± standard deviation. H, frozen-hydrated; D, frozen-dried; n, number of experiments.

for qualitative and quantitative analysis. Peaks from specimen holder, specimen stage, or microscope were not detected.

The techniques described permit x-ray microanalysis of frozen-hydrated sections in SEM. The availability of such techniques may permit wider use of this exciting analytical approach.

The authors wish to thank Mr. William Riley for his help and technical assistance throughout this study.

This project was supported by National Institutes of Health (NIH) grants GM 15904 and AM 18249. Dr. Beeuwkes is the recipient of NIH RCDA AM 00224 and a grant from R. J. Reynolds Industries, Inc.

Received for publication 3 December 1979, and in revised form 21 July 1980.

## REFERENCES

- Appleton, T. C. 1974. A cryostat approach to ultrathin "dry" frozen sections for electron microscopy: a morphological and x-ray analytical study. *J. Microsc. (Oxf.)*, 100:49-74.
- Bulger, R. E., R. Beeuwkes III, and A. J. Saubermann. 1981. Application of scanning electron microscopy to x-ray analysis of frozen-hydrated sections. III. Distribution of elements in the rat renal papilla. *J. Cell Biol.* 87:274-280.
- Cameron, I. L., N. K. R. Smith, and T. B. Pool. 1979. Element concentration changes in mitotically active and postmitotic enterocytes: an x-ray microanalysis study. *J. Cell Biol.* 80:444-450.
- Christensen, A. K. 1971. Frozen thin sections of fresh tissue for electron microscopy, with a description of pancreas and liver. *J. Cell Biol.* 51:772-804.
- Dörge, A., R. Rick, K. Gehring, J. Mason, and K. Thureau. 1975. Preparation and applicability of freeze-dried sections in the microprobe analysis of biological soft tissues. *J. Microsc. Biol. Cell.* 22:205-214.
- Echlin, P., H. le B. Skaer, B. O. C. Gardiner, F. Franks, and M. H. Asquith. 1977. Polymeric cryoprotectants in the preservation of biological ultrastructure. II. Physiological effects. *J. Microsc. (Oxf.)*, 110:239-257.
- Franks, F., M. H. Asquith, C. C. Hammond, H. le B. Skaer, and P. Echlin. 1977. Polymeric cryoprotectants. I. Low temperature states of aqueous solutions of hydrophilic polymers. *J. Microsc. (Oxf.)*, 110:223-238.
- Fuchs, W., J. D. Brombach, and W. Trosch. 1978. Charging effects in electron-irradiated ice. *J. Microsc. (Oxf.)*, 112:63-74.
- Gupta, B. L., T. A. Hall, and R. B. Moreton. 1977. Electron probe x-ray microanalysis. In *Transport of Ions and Water in Animals*. B. L. Gupta, R. B. Moreton, J. L. Oschman, and B. J. Wall, editors. Academic Press Inc. Ltd., London. 83-143.
- Hall, T. A. 1979. Biological x-ray microanalysis. *J. Microsc. (Oxf.)*, 117:145-163.
- Hall, T. A., H. C. Anderson, and T. Appleton. 1973. The use of thin specimens for x-ray microanalysis in biology. *J. Microsc. (Oxf.)*, 99:177-182.
- Hall, T. A., H. O. E. Rockert, and R. L. de C. H. Saunders. 1972. X-ray Microscopy in Clinical and Experimental Medicine. Charles C. Thomas, Publisher, Springfield, Ill. 161-162.
- Hodson, S., and J. Marshall. 1970. Ultracryotomy: a technique for cutting ultra thin sections of unfixed frozen biological tissues for electron microscopy. *J. Microsc. (Oxf.)*, 91:105-118.
- Hutchinson, T. E., M. Bacaner, J. Broadhurst, and J. Lilley. 1974. Instrumentation for direct microscopic elemental analysis of frozen biological tissue. *Rev. Sci. Instrum.* 45:252-255.
- Kronenberg, M. 1966. Thermal research in cutting metal. In *Machining Science and Application*. Pergamon Press, Oxford, England. 65-69.
- Moreton, R. B., P. Echlin, B. L. Gupta, T. A. Hall, and T. Weis-Fogh. 1974. Preparation of frozen hydrated tissue sections for x-ray microanalysis in the scanning electron microscope. *Nature (Lond.)*, 247:113-115.
- Saubermann, A. J. 1978. X-ray microanalysis of frozen hydrated tissue sections as a physiological tool. *Microsc. Acta*. (Suppl. 2):130-141.
- Saubermann, A. J., R. Beeuwkes III, and P. D. Peters. 1981. Application of scanning electron microscopy to x-ray analysis of frozen-hydrated sections. II. Analysis of standard solutions and artificial electrolyte gradients. *J. Cell Biol.* 87:268-273.
- Saubermann, A. J., R. Beeuwkes III, P. D. Peters, W. D. Riley, and R. E. Bulger. 1978. Definition of tissue compartments in renal papilla by direct x-ray microanalysis of frozen specimens. *Kidney Int.* 14:779.
- Saubermann, A. J., and P. Echlin. 1975. The preparation, examination and analysis of frozen hydrated tissue sections by scanning transmission electron microscopy and x-ray microanalysis. *J. Microsc. (Oxf.)*, 105:155-191.
- Saubermann, A. J., W. D. Riley, and R. Beeuwkes. 1977. Cutting work in thick section cryomicrotomy. *J. Microsc. (Oxf.)*, 111:39-49.
- Saubermann, A. J., W. D. Riley, and P. Echlin. 1977. Preparation of frozen hydrated tissue sections for x-ray microanalysis using a satellite vacuum coating and transfer system. *Scanning Electron Microsc.* 1:347-356.
- Schamber, F. H. 1977. A modification of the linear least-squares fitting method which provides continuum suppression. In *X-ray Fluorescence Analysis of Environmental Samples*. T. G. Dzubay, editor. Ann Arbor Science Publishers, Inc., Ann Arbor, Mich. 241-257.
- Shuman, H., A. V. Somlyo, and A. P. Somlyo. 1976. Quantitative electron probe microanalysis of biological thin sections: method and validity. *Ultramicroscopy*, 1:317-339.
- Sjöström, M., and L. E. Thornell. 1975. Preparing sections of skeletal muscle for transmission electron analytical microscopy (TEAM) of diffusible elements. *J. Microsc. (Oxf.)*, 103:101-112.
- Skaer, H. le B., F. Franks, M. H. Asquith, and P. Echlin. 1977. Polymeric cryoprotectants in the preservation of biological ultrastructure. III. Morphological aspects. *J. Microsc. (Oxf.)*, 110:257-270.
- Somlyo, A. V., H. Shuman, and A. P. Somlyo. 1977. Elemental distribution in striated muscle and the effects of hypertonicity. Electron probe analysis of cryosections. *J. Cell Biol.* 74:828-857.
- Somlyo, A. P., A. V. Somlyo, and H. Shuman. 1979. Electron probe analysis of vascular smooth muscle: composition of mitochondria, nuclei, and cytoplasm. *J. Cell Biol.* 81:316-335.
- Statham, P. J. 1978. Quantitative chemical analysis with EDS systems. In *Microbeam Analysis Society Proceedings Thirteenth Annual Conference*. K. F. J. Heinrich, editor. Microbeam Analysis Society. National Bureau of Standards, Washington, D. C. T2A-T2L.
- Talmon, Y., and E. L. Thomas. 1978. Electron beam heating temperature profiles in moderately thick cold stage STEM/SEM specimens. *J. Microsc. (Oxf.)*, 113:69-75.
- Trump, B. F., I. K. Berezsky, R. E. Pendergrass, S. H. Chang, R. E. Bulger, and W. J. Merguer. 1978. X-ray microanalysis of diffusible elements in scanning electron microscopy of biological thin sections. *Scanning Electron Microsc.* 2:1027-1039.